Improved modeling of sediment oxygen kinetics and fluxes in lakes and reservoirs

Xiamei Man[†], Kevin A. Bierlein[‡], Chengwang Lei[†], Lee D. Bryant[§], Alfred Wüest[‖,#], and John C. Little[‡*]

[†]Centre for Wind, Waves and Water, School of Civil Engineering, The University of Sydney, Sydney, NSW 2006, Australia

[‡]Department of Civil and Environmental Engineering, Virginia Tech, 401 Durham Hall, Blacksburg, Virginia, USA

[§]Department of Architecture and Civil Engineering, University of Bath, Bath, United Kingdom

[‖]Eawag, Swiss Federal Institute of Aquatic Science and Technology, Surface Waters – Research and Management, Kastanienbaum, Switzerland

[#] Physics of Aquatic Systems Laboratory, Margaretha Kamprad Chair, ENAC-IEE-APHYS, Swiss Federal Institute of Technology (EPFL), Lausanne, Switzerland

*Corresponding email: *jcl@vt.edu*

ABSTRACT

To understand water quality degradation during hypoxia, we need to understand sediment oxygen fluxes, the main oxygen sink in shallow hypolimnia. Kinetic models which integrate diffusion and consumption of dissolved oxygen (DO) in sediments usually assume a downward flux of DO from the sediment-water interface (SWI) with a zero-flux condition at the lower boundary of the oxic sediment layer. In this paper, we separately account for the oxidation of an upward flux of reduced compounds by introducing a negative flux of DO as a lower boundary condition. Using *in situ* measurements in two lakes, kinetic models were fit to DO microprofiles using zero-order and first-order kinetics with both zero and non-zero lower boundary conditions. Based on visual inspection and goodness-of-fit criteria, the negative-flux lower boundary condition, -0.25g O_2 $m^{-2}d^{-1}$, was found to more accurately describe DO consumption kinetics. Fitted zero-order rate constants ranged from 50 – 510 mg L^{-1} d^{-1} and first-order rate constants ranged from 60 – 400 d^{-1}, which agree well with prior laboratory studies. DO fluxes at the SWI calculated from the simulated

profiles with the negative-flux lower boundary condition also showed better agreement with the observed DO fluxes than the simulated profiles with the zero-flux lower boundary condition.

TOC ART

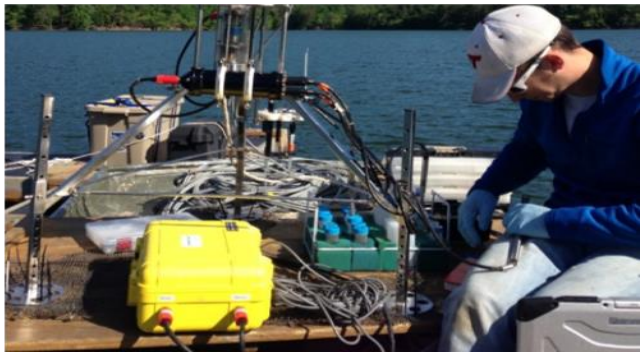

1.0 INTRODUCTION

Hypoxia, often defined as dissolved oxygen (DO) < 2 mg L^{-1}, commonly occurs in the deep waters of marine and freshwater systems during seasonal stratification[1]. In lakes and reservoirs, hypoxia usually leads to a lower redox potential in the sediments[2], which can result in the reduction and dissolution of ferric and manganese oxides, decreasing their capacity to adsorb and retain nutrients. As a result, the concentration of nutrients (*e.g.*, phosphorus and nitrogen) in the overlying water column increases[3-5] which may exacerbate blooms of nuisance algae and cyanobacteria[6-8]. Algal and cyanobacterial blooms are significant concerns for lake and reservoir management because they stimulate eutrophication[9], complicate water treatment processes and increase water treatment costs[10]. To make matters worse, some algae and cyanobacteria can be toxic[11] (*e.g.*, Karenia brevis), causing fish mortalities[9] and restricting tourism in coastal areas[12].

In the 1960s and 1970s, eutrophication stimulated by biologically available phosphorus was recognized as the primary cause of hypolimnetic hypoxia[13] in lakes and reservoirs. However, it was later discovered that simply preventing the release of phosphorous from the sediment by artificial aeration or oxygenation[10,14] did not eliminate hypolimnetic hypoxia as expected[15,16]. In some artificially oxygenated lakes, hypoxia was unaffected or even worsened[17] because DO was added to the water column but did not penetrate into the sediment, where reduced substances (*e.g.*, methane and ammonium) impacting hypolimnetic DO consumption are released[18]. Hypolimnetic DO demand and corresponding hypoxia are also influenced by DO consumption in the water column resulting from various chemical reactions and biological processes[19], such as settling of organic matter[20]. To better understand the processes governing hypolimnetic DO consumption, more attention should be paid to DO consuming processes in upper lacustrine sediment.

Sediment oxygen flux (J_{O2}) is usually the dominant sink for DO in the hypolimnion and usually comprises a majority of the DO demand in shallow water bodies. Processes on both sides of the sediment-water interface (SWI) influence J_{O2}[21]. On the water-side, J_{O2} is controlled by the presence of a diffusive boundary layer (DBL) immediately above the SWI. Molecular diffusion is the primary transport mechanism for DO through this thin, millimeter-scale layer, limiting the rate of DO transport to the SWI. Turbulent flow in the bottom boundary layer generally controls the thickness of the DBL (δ_{DBL}), and is therefore an important factor controlling J_{O2} from the water-

side of the SWI[22]. The concentration gradient of DO across the DBL also plays an important role, as it provides the driving force for diffusive transport. On the sediment-side of the SWI, DO may be transported deeper into the sediment porewater via diffusion or interstitial flow and is consumed within the sediments by aerobic microbial respiration and chemical oxidation of reduced species (*i.e.*, manganese, iron, ammonium and methane). Müller *et al.*[23] studied areal hypolimnetic mineralization (AHM) rates in 21 lakes in Switzerland and France and found that rates varied based on both sediment composition, depth of the hypolimnion and artificial oxygenation conditions. Under quiescent near-sediment flows, water-side processes typically limit J_{O2}[24]. Alternatively, sediment-side chemical and biological processes requiring DO can limit J_{O2} under turbulent conditions, when the supply of DO from the water column to the SWI exceeds the rate at which it can be consumed or transported deeper into the sediment[24]. In the hypolimnion of most lakes, turbulence near the SWI is low, meaning J_{O2} is primarily controlled on the water-side and DO is readily consumed within the upper few millimeters of sediment. In artificially oxygenated lakes and reservoirs, the oxygenation systems can enhance J_{O2} by increasing both turbulent mixing and DO concentrations near the SWI[25,26].

DO is consumed within the sediment by a broad range of processes driven by chemical and biological reactions. When simulating DO consumption within the sediment, these processes are usually lumped together into an apparent overall reaction rate, following zero-order, first-order, or Monod kinetics[19,22]. Prior studies have investigated the transport of DO in the sediment by fitting these kinetic models to DO microprofiles, or by measuring DO depletion rates in the water column above the sediment in different types of aquatic systems to calculate J_{O2} and estimate a rate constant. Brewer *et al.*[27] tracked DO concentrations in the water above a dredged sediment sample in laboratory incubations, assuming that DO consumption in the sediment followed first-order kinetics. Likewise, Beutel *et al.*[28] monitored DO depletion in sediment core incubations to calculate J_{O2}, also assuming first-order kinetics. Hall *et al.*[29] measured DO depletion rates using *in situ* flux chambers deployed in a Swedish fjord. They assumed zero-order kinetics, reporting a rate constant of 1750 mg L^{-1} d^{-1} (L refers to one litre of porewater in the sediment) at an *in situ* temperature of 10°C. Rasmussen and Jørgensen[21] incubated sediment cores collected from Aarhus Bay, Denmark, and measured DO microprofiles across the SWI using microsensors. They considered zero-order and first-order kinetic models, finding zero-order kinetics to fit the

98 microprofiles better than first-order. At an incubated temperature of 4°C, they reported a fitted
99 zero-order rate constant of 83 mg L^{-1} d^{-1}. House[30] used dredged riverine sediments in a laboratory
100 flume to measure factors affecting DO penetration into the sediment, including flow velocity above
101 the sediment, sediment grain size, and organic matter content. DO was measured in the water and
102 sediment using microsensors, similar to the Rasmussen and Jørgensen[22] study. House[30] considered
103 several kinetic models, including zero-order, first-order, and Monod kinetics. The study showed
104 that the simple zero-order model fit the data equally well or better than the more complex models.
105 Depending on the flow conditions above the SWI and the characteristics of the sediment, House
106 reported fitted zero-order rate constants ranging from 9.7 – 44 mg L^{-1} d^{-1} at an average temperature
107 of 18.4°C.
108
109 These studies, while informative and worthwhile, are all somewhat limited by their methods or
110 assumptions. A common approach is to only monitor DO in the water above the SWI[19,27,28].
111 However, this does not capture the behavior of DO within the sediment and does not capture
112 processes driving the kinetics and actual DO consumption within the sediment. Studies performed
113 on sediment in laboratory incubations[22,27,28,30] may disturb the sediment and SWI during the
114 dredging or coring process. Furthermore, laboratory conditions may not always be representative
115 of *in situ* conditions, particularly with respect to the critical control of turbulent flow in the water
116 overlying the sediment. The studies using microsensor measurements[22,30] assumed that DO
117 profiles were at steady state when fitting kinetic models to the data, which is appropriate for a
118 laboratory study under controlled conditions that allow the incubated sediment to reach steady
119 state. However, Bryant *et al*.[31] measured *in situ* DO microprofiles in a seiching lake and observed
120 large changes in the vertical DO distribution above the SWI and within the sediment on an hourly
121 timescale, highlighting the fact that ambient conditions in the field are typically quite variable and
122 that DO profiles in the sediment may never actually reach steady state.
123
124 Another key point is that almost all previous studies assumed zero-flux lower boundary conditions,
125 where the lower boundary was assumed to exist at the location where measurement terminated.
126 Interpretation of measured DO concentration profiles by Berg *et al.*[32] addresses this by accounting
127 for increased DO consumption in the upper sediment zone due to bioturbation; however, the
128 specific contribution of the reduced species flux was not considered.

A recent study that provides an innovative approach for upper sediment research is Müller *et al.*[23]. Combining water-column, sediment, and porewater chemistry analyses and sediment-to-water flux estimates in 11 eutrophic lakes, their study suggested a new method of describing sediment DO consumption close to the lower boundary. One main outcome of their research is to demonstrate that the estimated AHM rate (0.25 – 0.49 g O_2 m^{-2} d^{-1}) in eutrophic lakes is induced by both mineralization of organic material and a flux of reduced species propagating from the sediment towards the SWI including methane, ammonium, nitrate (NO_2^-), manganese (Mn(II)) and iron (Fe (II)). Their study is simplified compared to existing and more comprehensive models for sediment diagenesis[33], where the sediment is divided into an upper aerobic layer and a lower anaerobic layer. More comprehensive models simulate organic matter mineralisation, nitrification, denitrification, partitioning of hydrogen sulphide (H_2S) and oxidation, while the estimated AHM rate only considers the two most essential hypolimnetic DO depletion processes. Despite the simplification, the agreement between estimations and measurements of the AHM rates is striking. Although their study did not directly focus on sediment DO microprofiles, this has significant implications for the validity of the traditional sediment profile interpretation with the zero-flux boundary condition and also shows the potential to simplify the modeling of sediment DO kinetics by considering only the most essential biogeochemical processes impacting DO concentrations in the upper sediment.

This paper focuses on how to better describe DO consumption close to the lower boundary of the oxic freshwater sediments. Transient DO profiles are modeled under two different lower boundary conditions, but using the same governing equations. Simulated profiles with two lower boundary conditions are then compared to determine which lower boundary condition is more appropriate. Simulated sediment DO fluxes are also compared as they are critical parameters needed for defining water quality and ecosystem health for lake and reservoir management. To our knowledge, the current study is the first to fit kinetic models to obtain rate constants using DO microprofiles measured *in situ*, rather than using laboratory incubations. It is also the first kinetic study to consider the reaction of DO at the lower boundary with reduced species propagating upward from deeper within the sediments, inspired by Müller *et al.*[23]. In this study, the oxidation of the reduced species is assumed to be instantaneous at the bottom of the oxic sediment layer.

Although DO consumption within the oxic sediment layer is partially related to reduced species penetrating upward, there is evidence that the gradient of reduced species close to the bottom of the oxic layer is higher than in other regions of the upper sediment[34,35].

2.0 METHODS

2.1 Study Sites

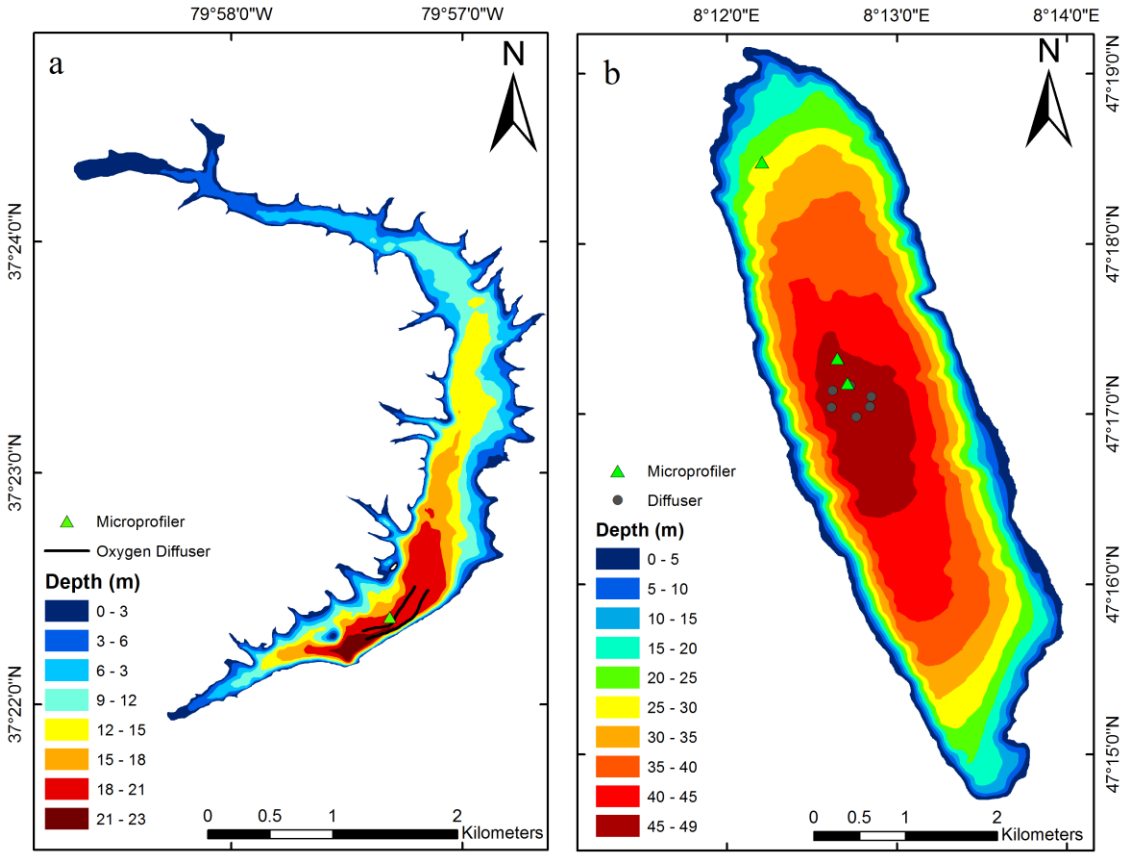

Figure 1. Bathymetric maps of (a) Carvins Cove Reservoir (CCR) and (b) Lake Hallwil (LH). Locations of the linear diffusers in CCR and the circular diffusers in LH are shown, as well as the deployed positions of the microprofiler. Note that one of the six diffuser symbols in LH is partially obscured by a symbol for the microprofiler.

DO microprofiles were measured *in situ* in two oxygenated lakes: Lake Hallwil and Carvins Cove Reservoir (Figure 1). Lake Hallwil (LH) is located north of Lucerne, Switzerland, on the Swiss

Plateau, and is primarily used for recreational purposes. It has a maximum depth of 48 m, a surface area of 9.95 km^2, a volume of 285×10^6 m^3 and is at an elevation of 449 m above mean sea level. Carvins Cove Reservoir (CCR) is a water-supply reservoir for the City of Roanoke in southwest Virginia, USA. CCR has a maximum depth of 22 m, a surface area of 2.5 km^2, a volume of 24×10^6 m^3 and is at an elevation of 357 m above mean sea level.

2.2 Microprofile Data Collection

A microprofiler (MP4; Unisense A/S) was deployed for periods of ~2 to ~5 days at three locations along the main axis of LH (as shown in Figure 1) from 24 May to 1 June 2012. The microprofiler was deployed at one location in CCR (also shown in Figure 1) from 26 May to 2 June 2013. While deployed, the microprofiler was equipped with a Clark-type oxygen microsensor (Unisense OX-100), as well as a thermocouple temperature sensor (Unisense TP-200). Measurements were made in triplicate at a sampling rate of 1 Hz at the following vertical resolution: 10 mm resolution from 100 mm to 10 mm above the SWI, 1 mm resolution from 10 mm to 5 mm above the SWI, and 0.1 mm resolution from 5 mm above the SWI to 5 mm below the SWI. The single oxygen microsensor was used to obtain three measurements in rapid succession at each vertical depth position; these triplicate measurements were averaged prior to modelling the data. This protocol resulted in complete microprofiles of both DO and temperature measured across the SWI every ~55 minutes.

The SWI location was visually determined by examining each microprofile to identify the linear region in the DBL and the slope change associated with the porosity difference between the water and sediment. The standard deviation of the triplicate DO measurements taken at each point in the microprofiles was used to further identify and confirm the correct location of the SWI, as standard deviation of DO measurements should decrease as the microsensor approaches the SWI[21].

2.3 Sediment Kinetics

Sediment DO kinetics is typically described using zero-order, first-order, or Monod (sometimes referred to as Michaelis-Menten) kinetic models. Zero-order and first-order kinetic models are shown below in equations 1 and 2[30]. These model formulations account for molecular diffusion of DO through the sediment porewater and consumption of DO within the sediment. Rather than trying to account for the numerous chemical and biological processes that consume DO in the

sediment, DO consumption is assumed to be adequately represented using an all-encompassing rate constant, or in the case of the Monod model, two constants. Monod kinetics have the effect of becoming zero-order or first-order depending on DO concentrations.

The study by House[30] showed that zero-order and Monod models described DO kinetics within the sediment equally well, although zero-order often agreed slightly better. Olinde[36] also showed that despite the additional fitting parameter offered by Monod kinetics, it does not result in a substantially improved fit to DO microprofiles measured during sediment core incubations. Given these observations and to minimize model complexity, the Monod kinetic model was not employed in this study. By applying a finite shift to the zero-order and first-order kinetic models (equations 1 and 2), the transient numerical solutions can be obtained (equations 3 and 4) as:

$$\frac{\partial C}{\partial t} = D_s \frac{\partial^2 C}{\partial z^2} - k_0 \quad (1)$$

$$\frac{\partial C}{\partial t} = D_s \frac{\partial^2 C}{\partial z^2} - k_1 C \quad (2)$$

$$\frac{C_n^i - C_n^{i-1}}{\Delta t} = \frac{D_s}{\Delta z^2}\left(C_{n+1}^{i-1} - 2C_n^{i-1} + C_{n-1}^{i-1}\right) - k_0 \quad (3)$$

$$\frac{C_n^i - c_n^{i-1}}{\Delta t} = \frac{D_s}{\Delta z^2}\left(C_{n+1}^{i-1} - 2C_n^{i-1} + C_{n-1}^{i-1}\right) - k_1 C_n^{i-1} \quad (4)$$

where C represents DO concentration, t is time, D_s is the effective diffusion coefficient of DO in the sediment (where $D_s = \varphi D_m$, φ is sediment porosity and D_m is the molecular diffusion coefficient of DO in water), z is depth below the SWI, k_0 is a zero-order rate constant, and k_1 is a first-order rate constant. The superscript i denotes the profile number in the time series of profiles, and the subscript n represents depth in the porewater DO profile, where the positive upward direction is towards the sediment.

The models were coded using Matlab[37]. They were initialized with the first profile in the series of microprofiles measured at each deployment, using only the portion of the profile at and below the SWI. Measured DO concentrations below 3 μmol L^{-1} were forced to zero, as concentrations below this level become difficult to discern from zero due to microsensor capabilities; furthermore, the depth at which DO is < 3 μmol L^{-1} (0.096 mg L^{-1}) has been defined as the depth of maximum DO penetration in previous studies (*e.g.*, Bryant *et al.*[35]). The model assumes constant temperature

234 over the series of profiles, as well as constant φ with sediment depth. This results in a constant
235 value of D_s for a given series of profiles. Measurements of φ were obtained from sediment cores
236 collected from both CCR and LH during field studies conducted prior to the current study,
237 following Dalsgaard *et al*[38]. The φ values in the sediment of CCR and LH were 0.96 and 0.94,
238 respectively[21]. The upper boundary condition is the measured DO concentration at the SWI. This
239 study adopts four methods of characterising boundary conditions, denoted by ZOZF, ZONF, FOZF
240 and FONF. ZOZF (zero-order, zero-flux) and ZONF (zero-order, negative-flux) adopt zero-order
241 kinetics, while FOZF (first-order, zero-flux) and FONF (first-order, negative-flux) adopt first-
242 order kinetics. The lower boundary condition for ZOZF and FOZF is the traditional zero-flux
243 boundary condition (equation 5) with the lower boundary located where the measurement
244 terminates (5 mm):
245
246 $$D_s \frac{\partial C}{\partial z} = 0\ g\ m^{-2} d^{-1} \quad (5)$$
247
248 The lower boundary condition for ZONF and FONF is a negative-flux boundary condition
249 (equation 6) with the lower boundary located where DO concentration goes to zero in each profile,
250 representing a fixed value of reduced species flux based on the general value Müller *et al*[23].
251 obtained for 11 eutrophic lakes:
252
253 $$D_s \frac{\partial C}{\partial z} = -0.25\ g\ m^{-2} d^{-1} \quad (6)$$
254
255 The benthic flux of reduced substance is set to a fixed value rather than being treated as a second
256 fitting parameter to ensure the stability of the kinetic model and to keep the model simple. Because
257 equations 1 and 2 are expressed in terms of DO, we assume that the upward flux of reduced
258 compounds is rapidly oxidized by DO and that the result could be reasonably expressed as an
259 upward "negative" flux of DO at the depth where the DO concentration becomes zero for each
260 profile. To ensure a stable solution that does not oscillate, the time-step (Δt) is made sufficiently
261 small so that the diffusion number (λ, equation 7) is less than 0.25[39].
262
263 $$\lambda = \frac{D_m \Delta t}{\Delta z^2} \quad (7)$$

Since the Δt necessary to achieve $\lambda < 0.25$ is much smaller than the time interval between two consecutive microprofiles measured in the field (Δt = 1 s in the model versus $\Delta t \approx 55$ min in field measurements), the DO concentration at the SWI used as the upper boundary condition for the modeled profiles is determined by linearly interpolating between measured DO concentrations at the SWI as needed. After the DO concentrations for every Δt (1 s) have been simulated, the DO concentration for the time between two microprofiles ($\frac{t^i + t^{i+1}}{2}$) is used as the simulated result of profile i, where t^i is the time when profile i starts being measured, and t^{i+1} is the time when profile i+1 starts being measured.

The models were evaluated using rate constants from 1 – 2000 (mg L^{-1} d^{-1} for zero-order kinetic models and d^{-1} for first-order kinetic models), whose range was selected based on reported values from previous studies[21,22,28,30]. The best-fit value for the kinetic rate constant is the value that minimizes the root mean square error (RMSE).

$$RMSE = \sqrt{\frac{\Sigma(C_{Obs} - C_{Sim})^2}{p}} \quad (8)$$

for each microprofile, where C_{Obs} is observed DO concentration, C_{Sim} is simulated DO concentration, and p is the total number of microprofile data points among all depths and profiles. After calculating the best-fit k_0 or k_1 for all profiles in one series, the average values of the best-fit k_0 and k_1 were applied as the best-fit kinetic rate constants for the full series of microprofiles; these globally averaged values were deemed most suitable due to the high variability in the profile-specific rate constants (as shown in Figure S5 – S8). The averaged best-fit k_0 and k_1 are used for additional analysis described in Section 2.4.

2.4 Model versus field data comparisons

Using the fitted k_0 and k_1 from each series of profiles, the sediment-side DO flux is calculated from the simulated profiles and compared to sediment-side DO flux calculated from the measured microprofiles. DO flux (J_{O2}) was estimated as:

$$J_{O2} = D_s \frac{\Delta C}{\Delta z} \quad (9)$$

where $\Delta C/\Delta z$ is the DO concentration gradient immediately below the SWI. To compare how well the modeled data agree with the field data, the relative error and the normalized RMSE are calculated using equations 10 and 11, where N is the number of profiles, $J_{O_2,Sim}$ is the simulated DO flux, $J_{O_2,Obs}$ is the observed DO flux, and the subscript *i* denotes profile number in the time series of profiles:

$$Relative\ error = \frac{J_{O_2,Sim_i} - J_{O_2,Obs_i}}{J_{O_2,Obs_i}} \quad (10)$$

$$Normalized\ RMSE = \sqrt{\frac{1}{N}\sum_{i=1}^{N}\left(\frac{J_{O_2,Sim_i} - J_{O_2,Obs_i}}{J_{O_2,Obs_i}}\right)^2} \quad (11)$$

3.0 RESULTS and DISCUSSION

3.1 Fitted Rate Constants

The fitted values of k_0 for ZOZF and ZONF, the fitted values of k_1 for FOZF and FONF, as well as the corresponding average RMSE values for each series of microprofiles, are displayed in Table 1. Values for k_0 and k_1 range from 120 – 510 mg L^{-1} d^{-1} and 90 – 400 d^{-1} in LH, while values for CCR are lower at 50 – 60 mg L^{-1} d^{-1} and 60 – 80 d^{-1}. Differences in the fitted rate constants between the two study sites are likely attributable to differences in the sediment composition between the two lakes, including the amount of labile organic matter and mineral composition. Labile carbon, reduced metals, and other chemical species exert a demand for DO within the sediment, and larger quantities of any of these oxygen-consuming species would result in an increase in the observed rate constant. The large range in fitted rate constants within LH is likewise attributable to spatial variability in sediment composition within LH itself. The first and third deployments were both in the central, deepest portion of LH (~42 m depth and ~300 m apart) and yielded similar best-fit rate constants. The second deployment, though still in the hypolimnion, was at a shallower location (~25 m depth) and has higher fitted rate constants. Sediment in the shallower portions of LH is likely to have more labile carbon in the sediment than deeper portions of the lake[21], since settling organic matter has less time to be oxidized in the water column before reaching the sediment. A similar observation was made in a study of Lake Gevena[40], a Swiss lake

where sediment DO uptake declines with increasing lake depth due to decreased rates of organic matter settling and sediment surface mineralization with greater depth. Additionally, the LH bubble-plume oxygenation system is located in the deepest portion of the lake, within 300 m of the first and third microprofiler deployments (LH – 1 and LH – 3, respectively). This oxygenation system, which has been in operation for roughly 30 years, would further enhance oxidation of settling organic matter in the water column by increasing the availability of DO in the water column, as well as by satisfying oxygen demand exerted by the nearby sediment. It has been shown that the organic content of sediment in LH has been significantly decreased by oxygenation[23,41]. Thus, it seems reasonable that the fitted rate constant should be higher in the shallower regions of the lake, which are also farther from the oxygenation system. Temperature may play a minor role in the increased best-fit rate constants at the shallower site, as temperatures measured near the SWI were only about 1°C warmer at this shallower location.

In both the CCR data set and the LH data sets, ZONF and FONF (with a negative-flux lower boundary condition) appear to fit much better than ZOZF or FOZF (zero-flux lower boundary condition) as evidenced by the distinctly lower RMSE values (Table 1). Most of the observed profiles also agree much better visually with the simulated profiles of ZONF and FONF than with those of ZOZF or FOZF in all data sets, as shown in Figures 2 and 3. It should be noted that in CCR, some profiles simulated by FOZF fit the field profiles very well while other profiles simulated by FOZF have rather high RMSEs, which is the reason why FOZF outperforms FONF in Table 2, but not Table 1. Considering this visual comparison and the relatively lower RMSE values, the negative-flux lower boundary condition appears to be more appropriate for describing DO consumption close to the lower boundary of the sediment for both LH and CCR. This provides strong evidence supporting the description of hypolimnetic DO consumption in the model of Müller *et al.*[23] Moreover, these new results indicate that it is possible to simulate DO consumption in the upper sediment by modeling the lumped zero-order or first-order reaction and the reduced species fluxes.

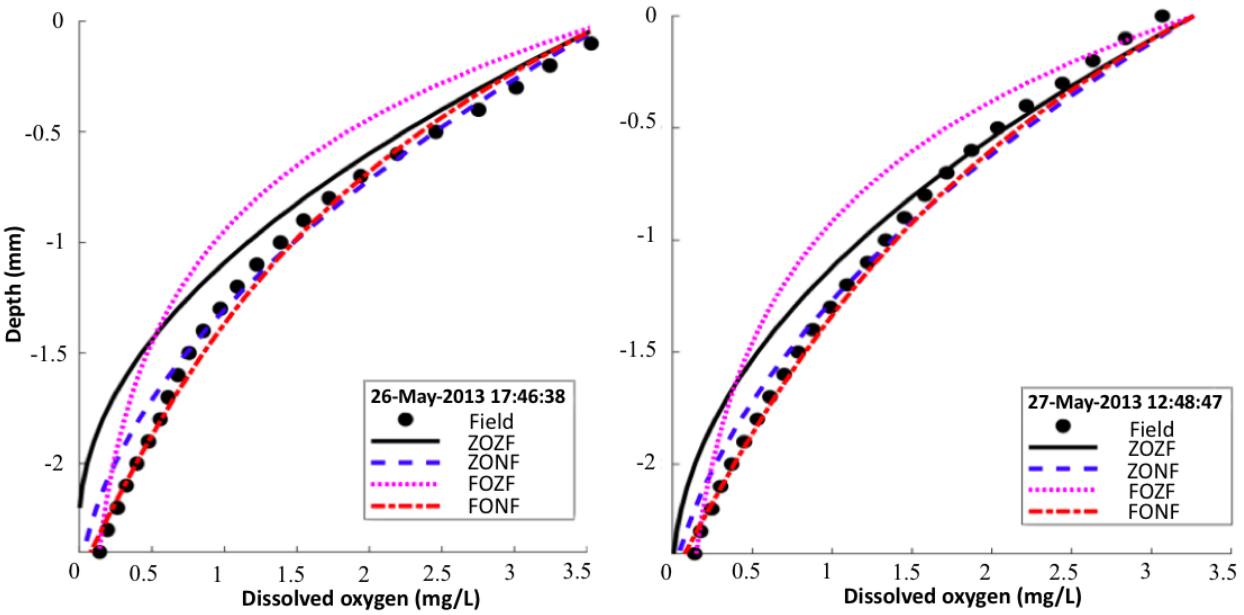

350

351 **Figure 2.** Characteristic DO microprofiles comparing field data to simulations by the four methods

352 (ZOZF, ZONF, FOZF, and FONF) in Carvins Cove Reservoir (CCR).

353

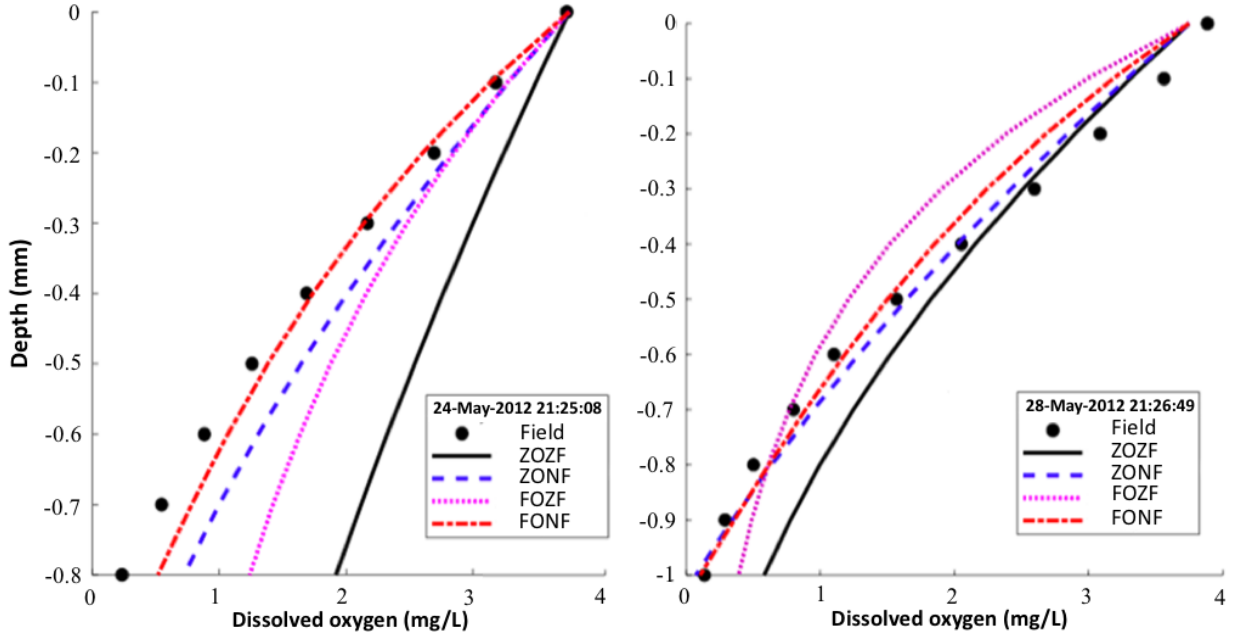

354

355 **Figure 3**. Characteristic DO microprofiles comparing field data to simulations by the four methods

356 (ZOZF, ZONF, FOZF, and FONF) in Lake Hallwil (LH).

357

Table 1. Summary of fitted kinetic rate constants and average root mean square error (RMSE) with lower RMSEs between ZOZF/ZONF and lower RMSEs between FOZF/FONF shown in bold.

		Zero-Order		First-Order	
		ZOZF	ZONF	FOZF	FONF
		k_0 (mg L^{-1} d^{-1})	k_0 (mg L^{-1} d^{-1})	k_1 (d^{-1})	k_1 (d^{-1})
CCR	Rate Constant	50	60	60	80
	RMSE (mg L^{-1})	0.32	**0.08**	0.30	**0.10**
LH-1	Rate Constant	150	170	90	130
	RMSE (mg L^{-1})	0.86	**0.37**	0.53	**0.38**
LH-2	Rate Constant	510	390	400	380
	RMSE (mg L^{-1})	0.58	**0.33**	0.54	**0.22**
LH-3	Rate Constant	200	120	190	120
	RMSE (mg L^{-1})	0.45	**0.14**	0.52	**0.13**
	RMSE average weighted by number of profiles in each data set (mg L^{-1})	0.46	0.17	0.41	0.16

Table 2. Percentage of each fitting method with the best performance among all 320 profiles (combined total for LH and CCR) based on RMSE value for each individual profile (higher percentages between ZOZF/ZONF and higher percentages between FOZF/FONF are shown in bold)

	ZOZF (%)	ZONF (%)	FOZF (%)	FONF (%)
CCR	13	**57**	**16**	14
LH-1	9	**23**	**23**	**45**
LH-2	13	**33**	11	**43**
LH-3	8	**47**	6	**39**

Differences between the simulated and observed profiles are likely a result of adopting the globally averaged rate constants and also the interpolation necessary to force the model. Since the field data only has direct DO measurements at the SWI roughly every 55 minutes, any fluctuation in DO concentrations at the SWI occurring on a shorter time scale are not represented in the model forcing. As mentioned in the methods section, the model time-step is one second (Δt = 1 s) to ensure stable solutions, which is much shorter than the ~55-min period between two consecutive *in situ* microprofiles. If higher frequency data were available to force the model, the agreement

between the simulated and observed profiles would likely improve. In some microprofiles (e.g., the profiles in Figure 2), the simulated DO concentration at depth = 0 mm is not equal to that of the observations. This is also related to interpolation of field profiles and reflects the time-consuming microprofile measurement process.

Despite some differences in the methods used for determining the best-fit rate constants, the fitted values generally compare quite well with the preliminary CCR study by Olinde[35]. Olinde found the best-fit k_0 to be 36 ± 10 mg L^{-1} d^{-1} at 4°C and 130 ± 66 mg L^{-1} d^{-1} at 20°C, while the best-fit k_1 was 34 ± 12 d^{-1} at 4°C and 170 ± 68 d^{-1} at 20°C. The fitted CCR values obtained in the current study (Table 2), measured at an *in situ* temperature of ~7.5°C agree nicely with the range from this preliminary study by Olinde[35].

Given the differences in methods and variable sediment composition and microbial community structure[43], the magnitude of the optimized zero-order rate constant for CCR agrees with k_0 reported by Rasmussen and Jørgensen[21] (83 mg L^{-1} d^{-1}) and House[28] (9.7 – 44 mg L^{-1} d^{-1}). The fitted k_0 for LH are higher than those reported by Rasmussen and Jørgensen[21] or House[28] but are still within a reasonable range; in comparison, Hall *et al.*[29] reported a k_0 that is an order of magnitude higher than those from LH (1750 mg L^{-1} d^{-1} versus 120 – 510 mg L^{-1} d^{-1}). It should also be taken into consideration that the negative-flux lower boundary condition in ZONF and FONF assumes an instantaneous reaction, while in natural water bodies the oxidation of reduced species is clearly not instantaneous but only gradually reduces the concentrations of reduced species over the distance of diffusion. Since the concentration gradient of reduced species in the upper sediments is extremely complex to characterize, the proposed simplification is reasonable but may lead to larger k_0 and k_1 estimates.

3.2 DO Flux Comparisons

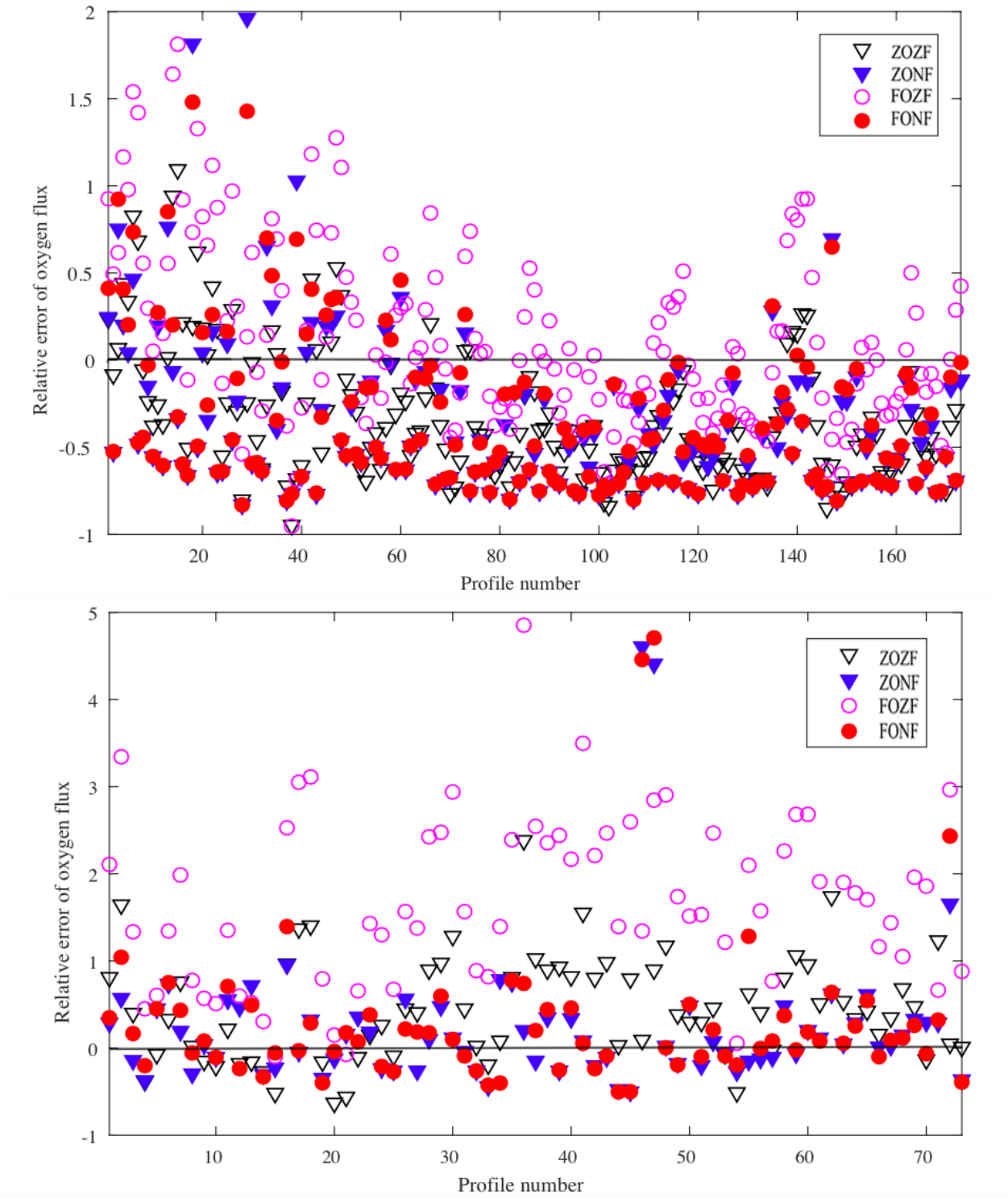

Figure 4. Relative error of the sediment-side DO fluxes at the sediment-water interface (SWI) in the CCR microprofiler deployment between 2013 May 26 and 2013 June 02

(upper plot) and the third microprofiler deployment in LH (LH – 3) between 2012 May 28 and 2012 June 01 (lower plot).

Sediment-side DO fluxes at the SWI calculated from the simulated DO profiles were used to estimate J_{O2}, which were then compared to field measurements. The first-order kinetics with zero-flux boundary condition (FOZF) typically overestimates the DO flux. The sediment-side DO flux calculated by negative-flux lower boundary conditions (ZONF, FONF) agrees better than zero-flux lower boundary conditions (ZOZF, FOZF) with the field data based on both visual inspection and the normalized RMSE values weighted by the number of profiles in each data set as shown in Figure 4 (and also Table S2 and Table S3). Due to the overestimation of FOZF, the normalized RMSE of DO flux calculated by FOZF is around twice the normalized RMSE of negative-flux lower boundary condition (ZONF, FONF) for both CCR and LH. This increased RMSE, along with Section 3.1 results, lend more support to using the negative-flux lower boundary condition over the zero-flux lower boundary condition when modeling DO flux on the sediment side of SWI in LH and CCR. In addition, ZONF seems to be the best method for LH, yielding the lowest RMSE. Another aspect to be considered is that Monod kinetics, a rate expression that is often used to describe microbial growth and single substrate degradation, have the effect of being zero-order when the concentration is much greater than the Monod half-saturation constant while being first-order when the concentration is much less than the half-saturation constant[39]. Because virtually all microbial DO consumption processes have a half-saturation constant near or below the detection limit of the microsensor[44] (3 μmol L^{-1}), it is not surprising that zero-order kinetics yield more reliable results.

DO fluxes at the SWI of some profiles have a normalized RMSE of more than 200%, which indicates that fluxes calculated from these simulated microprofiles, primarily by FOZF, do not adequately reproduce the actual measured fluxes. Müller *et al.*[23] assumed the reaction of DO with organic matter to be a first-order kinetic reaction, which indicates that the negative-flux lower boundary condition has only been studied and verified with first-order sediment kinetics. This may explain why FONF performs much better than FOZF while ZONF does not outperform ZOZF in DO flux comparison such as those discussed in Section 3.1. Additional sources of discrepancy may be due to the measured DO fluxes being subject to measurement errors at the SWI, especially

related to the determination of the exact SWI depth level, and the simulated DO fluxes being influenced by errors arising from the model and numerical solutions.

Both the simulated and observed sets of DO fluxes have significant implications for lake and reservoir management. The sediment-side DO fluxes are closely related to the water-side DO fluxes, which can also be derived from the kinetic rate constants based on empirical equations[19,25]. The comparison of the simulated and observed DO fluxes indicates that the simulated ones are more reliable than the observed ones because the simulated ones make use of all measured microprofiles. For these reasons, comprehensive microprofiling time-series paired with the model described in this study can provide a useful new tool in monitoring sediment DO fluxes for managing water quality and ecosystem health in lakes and reservoirs.

3.3 Limitation of the approach

A model of DO transport and consumption in freshwater sediments has been fit to DO microprofiles measured *in situ*, using zero-order and first-order kinetic models with zero-flux and negative-flux lower boundary conditions to determine the appropriate kinetic order and the appropriate bottom boundary condition. While the results support the inclusion of a flux of reduced species propagating upwards from deeper within the sediments, and thereby contributing to part of the overall sediment DO consumption and corresponding DO flux estimates, additional work is necessary. An even longer time-series of microprofiles may be obtained to make the analysis more robust. The overestimation of DO flux in some microprofiles is also likely to be a result of the interpolation necessary to force the model. With a higher-frequency data set to force the model, the agreement between observed and simulated microprofiles is expected to improve, which should, in turn, improve the fluxes calculated from the simulated profiles. If possible, placing focus on profiling immediately across the SWI and into the upper sediment (thereby excluding a majority of the overlying water column) would allow for considerably decreased profiling times, thereby minimising the difference between actual measurements and model time steps. In addition, the negative-flux value is fixed in this study; however, Müller *et al*.[23] suggested that values may vary among different lakes and even across different seasons and/or locations within the same lake. Further research is needed to better characterize the value of sediment DO fluxes in these complex aquatic systems using simplified, yet accurate models.

ASSOCIATED CONTENT

Supporting Information

The Supporting Information contains additional details on previous studies investigating DO kinetics in sediment porewater (Table S1), comparison between normalized RMSE of DO flux using the four methods (ZOZF, ZONF, FOZF, and FONF; Table S2), percentage of profiles whose sediment-side DO flux have relative error less than ±0.5 and ±1.0 (Table S3), DO concentration at the SWI for each site (Figure S1 – S4), kinetic rate constants of each profile for each site (Figures S5 – S8), in situ and simulated DO profiles by ZOZF, ZONF, FOZF and FONF in CCR and LH (Figure S9 – S169).

AUTHOR INFORMATION

Corresponding Author

*E-mail: jcl@vt.edu; Phone: (540) 231 0836.

ORCID

Lee D. Bryant: 0000-0002-1783-6942

Chengwang Lei: 0000-0002-8175-4781

John C. Little: 0000-0003-2965-9557

Alfred Wüest: 0000-0001-7984-0368

Notes

The authors declare no competing financial interest.

ACKNOWLEDGEMENTS

This research was primarily supported by U.S. National Science Foundation grant CBET 1033514. We would like to thank the Western Virginia Water Authority for access to Carvins Cove Reservoir and Kanton Aargau for access to Lake Hallwil during the field campaigns. We also are grateful to Michael Schurter of Eawag, Arno Stöckli of Kanton Aargau, Scott Socolofsky and Maryam Rezvani of Texas A&M University, and Christina Urbanczyk for their valuable assistance during the field campaigns.

REFERENCES

1. Conley, D. J.; Björke, S.; Bonsdorf, E.; Carstensen, J.; Destouni, G.; Gustafsson, B. G.; Hietanan, S.; Kortekaas, M.; Kuosa, H.; Meier, H. E. M.; Müller-Karulis, B.; Nordberg, K.; Norkko, A.; Nürnberg, G.; Pitkänen, H.; Rabalais, N. N.; Rosenberg, R.; Savchuk, O. P.; Slomp, C.P.; Voss, M.; Wulff, F.; Zillén, L. Hypoxia-related processes in the Baltic Sea. *Environ. Sci. Technol*. **2009**, 43 (10), 3412-3420.
2. Li, Q.; Bi, S.; Ji, G. Determination of strongly reducing substances in sediment. *Environ. Sci. Technol*. **2003**, 37 (24), 5727-5731.
3. Beutel, M. W.; Leonard, T. M.; Dent, S. R.; Moore, B. C.; Effects of aerobic and anaerobic conditions on P, N, Fe, Mn, and Hg accumulation in waters overlaying profundal sediments of an oligo-mesotrophic lake. *Water Res*. **2008**, 42 (8-9), 1953-1962.
4. Huttunen, J. T.; Väisänen, T. S.; Hellsten, S. K.; Martikainen, P. J. Methane fluxes at the sediment-water interface in some boreal lakes and reservoirs. *Boreal Environ. Res*. **2006**, 11 (1) 27-34.
5. Davison, W. Iron and manganese in lakes. *Earth Sci. Rev*. **1993**, 34, 119-163.
6. Wang, H.; Dai, M.; Liu, J.; Kao, S.; Zhang, C.; Cai, W.; Wang, G.; Qian, W.; Zhao, M.; Sun, Z. Eutrophication-driven hypoxia in the East China Sea off the Changjiang Estuary. *Environ. Sci. Technol*. **2016**, 50, (5), 2255-2263.
7. Funkey, C. P.; Conley, D. J.; Reuss, N. S.; Humborg, C.; Jilbert, T.; Slomp, C. P. Hypoxia sustains cyanobacteria blooms in the Baltic Sea. *Environ. Sci. Technol*. **2014**, 48 (5), 2598-2602.
8. Gao, Y.; Cornwell, J. C.; Stoecker, D. K.; Owens, M. S. Influence of cyanobacteria blooms on sediment biogeochemistry and nutrient fluxes. *Limnol. Oceanogr*. **2014**, 59 (3), 959-971.
9. Wu, R. S. S.; Zhou, B. S.; Randall, D. J.; Woo, N. Y. S.; Lam, P. K. S. Aquatic hypoxia is an endocrine disruptor and impairs fish reproduction. *Environ. Sci. Technol*. **2003**, 37 (6), 1137-1141.
10. Gantzer, P. A.; Bryant, L. D.; Little, J. C. Controlling soluble iron and manganese in a water-supply reservoir using hypolimnetic oxygenation. *Water Res*. **2009**, 43 (5), 1285-1294.
11. Cheng, Y. S.; McDonald, J. D.; Kracko, D.; Irvin, C. N.; Zhou, Y.; Pierce, R. H.; Henry, M. S.; Bourdelaisa, A.; Naar, J.; Baden D. G. Concentration and particle size of airborne toxic algae (Brevetoxin) derived from ocean read tide events. *Environ. Sci. Technol*. **2005**, 39 (10), 3443-3449.
12. Trottet, A.; Wilson, B.; Xin, G. S. W.; George, C.; Casten, L.; Schmoker, C.; Rawi, N. S. B. N.; Siew, M. C.; Larsen, O.; Eikaas, H. S.; Tun, K.; Drillet, G. Resting stage of plankton diversity from Singapore coastal water: Implications for harmful algae blooms and coastal management. *Environ. Manage.* **2018**, 61 (2),275-290.
13. Schindler, D. W.; Carpenter, S. R.; Chapra, S. C.; Hecky, R. E.; Orihel, D.M. Reducing phosphorus to curb lake eutrophication is a success, *Environ. Sci. Technol*. **2016**, 50 (17), 8923-8929.
14. Singleton, V. L.; Little, J. Designing hypolimnetic aeration and oxygenation systems – A review. *Environ. Sci. Technol*. **2006**, 40 (24), 7512-7520.
15. Kleeberg, A.; Herzog, C.; Hupfer, M. Redox sensitivity of iron in phosphorus binding does not impede lake restoration. *Water Res*. **2013**, 47 (3), 1491-1502.
16. Testa, J. M.; Kemp, W. M. Hypoxia-induced shifts in nitrogen and phosphorus cycling in Chesapeake Bay. *Limnol. Oceanogr*. **2012**, 57 (3), 835-850.

17. Gächter, R.; Wehrli, B. Ten years of artificial mixing and oxygenation: no effect on the internal phosphorus loading of two eutrophic lakes. *Environ. Sci. Technol*. 1998, 32, 3659-3665.
18. Matzinger, A.; Müller, B.; Niederhauser, P.; Schmid, M.; Wüest, A.; Hypolimnetic oxygen consumption by sediment-based reduced substances in former eutrophic lakes. *Limnol. Oceanogr*. **2010**, 55, 2073-2084.
19. Higashino, M.; Gantzer, C.; Stefan, H. Unsteady diffusional mass transfer at the sediment/water interface: Theory and significance for SOD measurement. *Water Res*. **2004**, 38 (1), 1-12.
20. Beutel M. W. Hypolimnetic anoxia and sediment oxygen demand in California drinking Water Reservoirs, *Lake. Resevir. Manage.,* **2003**, 19 (3), 208-221, DOI: 10.1080/07438140309354086
21. Bryant, L. D.; McGinnis, D. F.; Lorrai C.; Brand A.; Little J. C.; Wüest A. Evaluating oxygen fluxes using microprofiles from both sides of the sediment-water interface, *Limnol. Oceanogr. Methods*, **2010a**, 8, 610-627. doi:10.4319/lom.2010.8.0610.
22. Rasmussen, H.; Jørgensen, B. B. Microelectrode studies of seasonal oxygen uptake in a coastal sediment: role of molecular diffusion. *Mar. Ecol. Pro. Ser*. **1992**, 81 (3), 289-303.
23. Müller, B.; Bryant, L. D.; Matzinger, A.; Wüest, A. Hypolimnetic oxygen depletion in eutrophic lakes. *Environ. Sci. Technol*. **2012**, 46 (18), 9964-9971.
24. O'Connor, B.; Hondzo, M.; and Harvey, J. Incorporating both physical and kinetic limitations in quantifying dissolved oxygen flux to aquatic sediments. *J. Environ. Eng*. **2009**, 135 (12), 1304-1314.
25. Bierlein, K. A.; Rezvani, M..; Socolofsky, S. A.; Bryant, L. D.; Wüest, A.;Little, J. C. Increased sediment oxygen flux in lakes and reservoirs: The impact of hypolimnetic oxygenation. *Water Resour. Res*. **2017**, 53 (6), 4876-4890, doi:10.1002/2016WR019850
26. Larsen, S. J.; Kilminster, K. L.; Mantovanelli, A.; Goss, Z. J.; Evans, G. C.; Bryant, L. D.; McGinnis D. F. Artificially oxygenating the Swan River estuary increases dissolved oxygen concentrations in the water and at the sediment interface. *Ecol. Eng*. **2019**, 128, 112-121
27. Brewer, W,; Abernathy, A. R.; Paynter, M. J. B. Oxygen consumption by freshwater sediments. *Water Res*. **1977**, 11 (5), 471-473.
28. Beutel, M.; Hannoun, I.; Pasek, J.; Kavanagh, K. B. Evaluation of hypolimnetic oxygen demand in a large eutrophic raw water reservoir, San Vicente Reservoir, Calif. *J. Environ. Eng*. **2007**, 133 (2), 130-138.
29. Hall, P. O. J.; Anderson, L. G.; van der Loeff, M. M. R.; Sundby, B.; Westerlund, S. F. G. Oxygen uptake kinetics in the benthic boundary layer. *Limnol. Oceanogr*. **1989**, 34 (4), 734-746.
30. House, W. Factors influencing the extent and development of the oxic zone in sediments. *Biogeochem*. **2003**, 63 (3), 317-334.
31. Bryant, L. D.; Lorrai, C.; McGinnis, D. F.; Brand, A.; Wüest, A.; Little, J. C. Variable sediment oxygen uptake in response to dynamic forcing. *Limnol. Oceanogr*. **2010b**, 55 (2), 950-964.
32. Berg, P.; Risgaard-Petersen, N.; Rysgaard, S. Interpretation of measured concentration profiles in sediment pore water. *Limnol. Oceanogr*. **1998**, 43(7), 1500-1510.
33. Brady, D. C.; Testa, J. M; Di Toro, D. M.; Boynton, W. R.; Kemp, W. M. Sediment flux modelling: Calibration and application for coastal systems, *Est. Coa. She. Sci*. **2013**. 117, 107- 124.
34. Kristensen, E.; Hansen, T.; Matthieu, D.; Banta, G.T.; Cintia, C. Q. Contrasting effects of the polychaetes Marenzelleris viridis and Nereis diversicolor on benthic metabolism and solute transport in coastal sediment, *Mar. Ecol. Prog. Ser.* **2011**, 425, 125-139.

588 35. Bryant, L. D.; Hsu-Kim, H.; Gantzer, P. A.; Little, J.C. Solving the problem at the source:
589 Controlling Mn release at the sediment-water interface via hypolimnetic oxygenation. *Water Res*.
590 **2011**, 45(19), 6381–6392. https://doi.org/10.1016/j.watres.2011.09.030
591 36. Olinde, L. J. Sediment oxygen demand kinetics, Master's Thesis, Virginia Polytechnic
592 Institute and State University. **2007**
593 37. MATLAB and Statistics Toolbox Release 2014, The MathWorks, Inc., Natick,
594 Massachusetts, United States.
595 38. Bryant, L. D.; P. A. Gantzer.; Little, J. C. Increased sediment oxygen uptake caused by
596 oxygenation-induced hypolimnetic mixing. *Water Res*. **2011**, 45 (12), 3692-3703.
597 39. Dalsgaard, T.; Nielsen L. P.; Brotas, V.; Viaroli, P.; Underwood, G.; Nedwell, D. B.;
598 Sundbäck, K.; Rysgaard, S.; Miles, A.; Bartoli, M.; Dong, L.; Thornton, D. C. O.; Ottosen, L. D.
599 M.; Castaldelli, G.; Risgaard-Petersen, N. **2000**. Protocol Handbook for NICE – Nitrogen Cycling
600 in Estuaries: A Project under the EU Research Programme: Marine Science and Technology
601 (MAST). National Environmental Research Institute, Silkeborg, Denmark.
602 http://www2.dmu.dk/LakeandEstuarineEcology/nice/NICE_handbook.pdf
603 40. Chapra, S. C. Surface water-quality modeling. McGraw-Hill, Boston, Mass, USA. **1997**,
604 pg 214.
605 41. Schwefel, R.; Steinsberger, T.; Bouffard, D., Bryant, L.; Müller, B.; Wüest, A. Using
606 small-scale measurements to estimate hypolimnetic oxygen depletion in a deep lake. *Limnol.*
607 *Oceanogr*. **2018**, 63 (S1), S54–S67. https://doi.org/10.1002/lno.10723
608 42. Liu, C.; Zachara, J. M. Uncertainties of monod kinetics parameters nonlinearly estimated
609 from batch experiments. *Environ. Sci. Technol*. **2001**, 35 (1), 133-141.
610 43. Bryant, L. D.; Little, J. C.; Bürgmann, H. Response of sediment microbe community
611 structure in a freshwater reservoir to manipulations in oxygen availability. FEMS Microbiol. Ecol.
612 2012, 80, 248-263. http://doi.org/10.1111/j.1574-6941.2011.01290.x
613 44. Stadler , L. B.; Love, N. G. Oxygen half-saturation constants for pharmaceuticals in
614 activated sludge and microbial community activity under varied oxygen levels. *Environ. Sci.*
615 *Technol*. **2019**, 53 (4), 1918-1927.